

LETTER • OPEN ACCESS

Decadal changes in rapid intensification of western North Pacific tropical cyclones modulated by the North Pacific Gyre Oscillation

To cite this article: Jinjie Song *et al* 2023 *Environ. Res. Commun.* **5** 071005

View the [article online](#) for updates and enhancements.

You may also like

- [The warm Blob in the northeast Pacific—the bridge leading to the 2015/16 El Niño](#)
Yu-Heng Tseng, Ruiqiang Ding and Xiaomeng Huang
- [The zonal North Pacific Oscillation: a high-impact atmospheric teleconnection pattern influencing the North Pacific and North America](#)
Anran Zhuge and Benkui Tan
- [Enhanced mid-to-late winter predictability of the storm track variability in the North Pacific as a contrast with the North Atlantic](#)
Yu Nie, Hong-Li Ren and Adam A Scaife

Environmental Research Communications



LETTER

Decadal changes in rapid intensification of western North Pacific tropical cyclones modulated by the North Pacific Gyre Oscillation

OPEN ACCESS

RECEIVED

24 April 2023

REVISED

28 June 2023

ACCEPTED FOR PUBLICATION


13 July 2023

PUBLISHED

28 July 2023

Original content from this work may be used under the terms of the [Creative Commons Attribution 4.0 licence](https://creativecommons.org/licenses/by/4.0/).

Any further distribution of this work must maintain attribution to the author(s) and the title of the work, journal citation and DOI.

Jinjie Song^{1,2} , Philip J Klotzbach³, Yifei Dai^{1,2} and Yihong Duan^{2,*}¹ Nanjing Joint Institute for Atmospheric Sciences, Chinese Academy of Meteorological Sciences, Nanjing, People's Republic of China² State Key Laboratory of Severe Weather, Chinese Academy of Meteorological Sciences, Beijing, People's Republic of China³ Department of Atmospheric Science, Colorado State University, Fort Collins, CO, United States of America

* Author to whom any correspondence should be addressed.

E-mail: duanyh@cma.gov.cn**Keywords:** tropical cyclone, rapid intensification, North Pacific Gyre Oscillation**Abstract**

This study investigates the modulation of western North Pacific (WNP) tropical cyclone rapid intensification (RI) by the North Pacific Gyre Oscillation (NPGO) on decadal timescales. There is a significant inverse relationship between basinwide RI numbers during July–November and the simultaneous NPGO index from 1970 to 2021. During the positive NPGO phase, suppressed RI occurs over almost the entire WNP, with a distinctly different spatial distribution compared to the Pacific Decadal Oscillation-driven pattern of RI modulation. RI occurrence is significantly reduced over the eastern Philippine Sea (10°–25°N, 140°–155°E). This is primarily caused by enhanced negative low-level vorticity, which can be linked to the horizontal extent of the anomalous low-level anticyclone. By comparison, over the western Philippine Sea (10°–25°N, 125°–140°E), there are only weak RI occurrence changes due to offsetting influences of increased mid-level humidity and decreased low-level vorticity.

1. Introduction

Rapid intensification (RI) is generally considered to be a sharp increase in tropical cyclone (TC) intensity during a short timespan. The canonical definition of RI is often taken to be a maximum sustained wind increase of at least 30 kt over a 24-h period (Kaplan and DeMaria, 2003). RI is particularly difficult to simulate and predict, consequently posing great challenges for operational TC forecasting (Knaff *et al* 2018). Given increasing concerns about climate change and its impacts on TC activity, there has been heightened attention paid to temporal changes in RI (Walsh *et al* 2016). In particular, several studies have examined RI variability on various timescales over the western North Pacific (WNP), which climatologically has more frequent RI events than any other global TC basin (Lee *et al* 2016).

El Niño–Southern Oscillation (ENSO) is one of the primary factors modulating RI over the WNP on interannual timescales. WNP RI activity is enhanced in El Niño years and is suppressed in La Niña years. The El Niño enhancement has been attributed to an RI-favorable environment driven by a strengthened and southeastward-extended monsoon trough over the WNP (Wang and Zhou, 2008, Fudeyasu *et al* 2018). Additionally, different El Niño flavors can lead to distinct changes in various TC metrics, including RI number, the ratio of RI cases to total TC cases, and RI occurrence position (Shi *et al* 2020, Guo, Tan 2021).

On decadal-to-multidecadal timescales, WNP RI variability has been linked to phase changes of the Pacific Decadal Oscillation (PDO) (Wang *et al* 2015, Zhao *et al* 2018, Zhang *et al* 2020, Chu and Murakami, 2022). The PDO has been defined as the first empirical orthogonal function (EOF) of North Pacific (20°–70°N) sea surface temperature (SST) anomalies (SSTAs) (Mantua *et al* 1997, Newman *et al* 2016). Wang *et al* (2015) found that during the warm (cold) PDO phase, the annual RI number was, on average, lower (higher), and the average RI occurrence position migrated southeastward (northwestward). Zhao *et al* (2018) and Zhang *et al* (2020) both

found a significantly larger proportion of TCs experiencing RI to the total number of TCs during the cold PDO phase than during the warm PDO phase. During the cold PDO phase, easterly trade winds increased at low levels, leading to a steeper thermocline slope that hampered eastward migration of warm water in the equatorial Pacific. Simultaneously, more warm equatorial water spread northward into the main RI region via enhanced meridional ocean advection associated with Ekman transport. This consequently resulted in an oceanic environment with greater TC heat potential (TCHP) and warmer SSTs, favoring RI development (Wang *et al* 2015, Zhao *et al* 2018, Zhang *et al* 2020).

The North Pacific Gyre Oscillation (NPGO) has been defined as the second EOF of Northeast Pacific (180° – 110° W, 25° – 62° N) sea surface height anomalies (Di Lorenzo *et al* 2008). This definition of the NPGO is also consistent with the second EOF of North Pacific SSTAs (Bond and Harrison, 2000). Chhak *et al* (2009) found that the North Pacific Oscillation (NPO) was the atmospheric forcing pattern of the NPGO, which is characterized by a north-south dipole sea level pressure pattern over the North Pacific (e.g., Rogers, 1981). In addition, Bond *et al* (2003) showed that the North Pacific SSTA footprint of the NPGO was identical to the Victoria Mode (VM) that exhibited a northeast-southwest oriented dipole SST pattern over the North Pacific.

The physical mechanisms of the NPGO still remain elusive. Chhak *et al* (2009) reported that the NPGO was mainly driven by the NPO, with the NPGO pattern mainly being forced by anomalous horizontal advection of mean SST and vertical advection via Ekman pumping. Di Lorenzo *et al* (2010) argued that the NPGO was an oceanic expression on decadal timescales to the low frequency extratropical atmospheric forcing excited by central Pacific ENSO, while the PDO was primarily linked to eastern Pacific ENSO. Sullivan *et al* (2016) pointed out that the central Pacific ENSO showed a major spectral peak at around 10 years, with comparatively weak power on interannual timescales. The NPGO power spectrum exhibited enhanced variance at ~ 10 -yr (Yi *et al* 2015), which was shorter than the preferred period of the PDO.

A few studies have discussed the decadal modulation of WNP TC activity by the NPGO. Zhang *et al* (2013) found a significant inverse relationship between the NPGO index and basinwide WNP TC frequency. They attributed this relationship to negative relative vorticity anomalies over most of the WNP and strong vertical wind shear (VWS) east of 150° E during positive NPGO phases. Via partial correlation analysis, Zhang *et al* (2013) showed that the NPGO had a much closer association with WNP TC frequency than the PDO. Moreover, Dai *et al* (2022) found a west-east dipolar pattern of decadal changes in TC formation driven by the NPGO, with strongly suppressed (weakly enhanced) TC formation east (west) of 140° E during positive NPGO phases. This pattern could be linked to NPGO-induced changes in vertical motion and VWS over the western and eastern parts of the WNP, respectively.

It remains unclear whether changes in RI over the WNP are modulated by the NPGO. The PDO and the NPGO are often considered as the two leading EOFs of Pacific decadal variability (Di Lorenzo *et al* 2008), indicating that their temporal variations are linearly independent of each other as a result of their orthogonality. Consequently, it is very likely that NPGO-induced RI changes are distinct from the aforementioned RI changes induced by the PDO. In addition, the PDO power spectrum shows multidecadal peaks, particularly for periods of ~ 20 and ~ 70 years (Newman *et al* 2016), while the NPDO exhibits a significant spectral peak at ~ 10 years (Ding *et al* 2015). This means that the NPGO can influence WNP RI activity on shorter timescales than the PDO. Third, the variance and amplitude of the NPGO have increased since 1950, and are generally comparable to the PDO (Litzow *et al* 2020, Dong *et al* 2022). The fraction of Pacific SST variability contributed by the NPGO has increased, with the NPGO surpassing the PDO as the dominant mode of North Pacific SST variability since the 1990s (Bond *et al* 2003, Litzow *et al* 2020). This implies that decadal changes in WNP RI during recent decades may be more linked to the NPGO than the PDO.

Given these hypotheses, we investigate the response of WNP RI to the NPGO on decadal timescales. After excluding the PDO influence, we show how the NPGO affects spatiotemporal variations in WNP RI through modulation of the large-scale environment. The remainder of this study is arranged as follows. Section 2 discusses the TC and environmental datasets employed as well as the specific methodology used for the analysis. Section 3 compares spatiotemporal variations in WNP RI events driven by the PDO and the NPGO. Section 4 focuses on how the NPGO modulates changes in several environmental conditions. This study concludes with a summary in section 5.

2. Data and methods

This study uses 6-hourly TC best track data from the Joint Typhoon Warning Center (JTWC) as archived in the International Best Track Archive for Climate Stewardship (IBTrACS) v04r00 (Knapp *et al* 2010). There are systematic overestimates in TC intensity from the JTWC best track data during the pre-satellite era, which are caused by inconsistent and changing measurement technologies and reporting practices (Emanuel 2000). Hence this study focuses on the period of 1970–2021, as an increasing fraction of intensity estimates have been obtained

entirely through satellite data since the 1970s (Emanuel 2000). Several previous publications have used 1970 as a starting year for analyzing WNP TC activity (e.g., Emanuel, 2000, Kowch and Emanuel 2015, Wu *et al* 2020). This 52-yr time period is sufficient to reveal RI-related decadal variations, given that the NPGO's spectrum peaks at ~ 10 years (Ding *et al* 2015). Other studies have also investigated decadal changes in WNP TC activity using data since 1970 (e.g., Wu *et al* 2020).

Similar to previous publications (e.g., Kaplan and DeMaria 2003, Kaplan *et al* 2010, Shu *et al* 2012, Knaff *et al* 2018), an RI event is defined as a 24-h overwater change of at least 30 kt in 1-min maximum sustained wind. These RI events are identified in 6-h intervals, so a TC may experience more than one RI event during its lifetime. This study focuses on RI events over the WNP (north of the equator and 100°E – 180°). Additionally, RI activity is investigated during July–November (JASON), which includes 84% of RI events that occurred over the entire year (Wang and Zhou 2008, Ge *et al* 2018). Several prior studies have used other 24-h intensity change thresholds for identifying WNP RI, such as 35 kt (Lee *et al* 2016), 45 kt (Li *et al* 2022) and 50 kt (Song *et al* 2020). The decadal changes in WNP RI number identified using different thresholds are very similar, as are their relationships with the PDO and the NPGO (figures not shown).

Favorable large-scale environmental conditions are critical for the occurrence of RI, including high maximum potential intensity (MPI), high TCHP, large depth-averaged ocean temperature (DAT) from the surface to 100 m, a moist lower-to-middle troposphere, a low-level cyclonic circulation, upper-level divergent flow, and low VWS (Price 2009, Shu *et al* 2012, Fudeyasu *et al* 2018, Knaff *et al* 2018, Qin *et al* 2023, Wang *et al* 2023). These environmental variables are calculated from the Hadley Centre Sea Ice and Sea Surface Temperature dataset (HadISST; Rayner *et al* 2003), the fifth generation European Centre for Medium-Range Weather Forecasts (ECMWF) reanalysis of the global climate (ERA5; Hersbach *et al* 2020) and the control member of the ECMWF Ocean Reanalysis System 5 (ORAS5; Zuo *et al* 2019), with resolutions of $1^{\circ} \times 1^{\circ}$, $0.25^{\circ} \times 0.25^{\circ}$ and $1^{\circ} \times 1^{\circ}$, respectively. We re-grid the ERA5 data onto a $1^{\circ} \times 1^{\circ}$ grid to match the resolutions of HadISST and ORAS5. Note that HadISST and ERA5 provide the primary forcing fields for ORAS5, leading to physical consistency between these datasets (Zhuo *et al* 2019). In addition, JASON averages of the PDO and NPGO indices are obtained from the National Oceanic and Atmospheric Administration's Earth System Research Laboratory Physical Sciences Division.

We use partial correlation and partial regression methods to derive the linear relationship between two variables after excluding the linear influence of the third variable. This approach has been widely utilized in the climate research community (e.g., Saji and Yamagata 2003, Cai *et al* 2011, Ham *et al* 2013, Kim *et al* 2020, Zhu *et al* 2022). The partial correlation is computed as:

$$r_{12,3} = \frac{r_{12} - r_{13}r_{23}}{\sqrt{(1 - r_{13}^2)(1 - r_{23}^2)}}, \quad (1)$$

where r_{12} , r_{13} and r_{23} refer to the Pearson correlation coefficients between any two of the three variables. The partial regressions are calculated using:

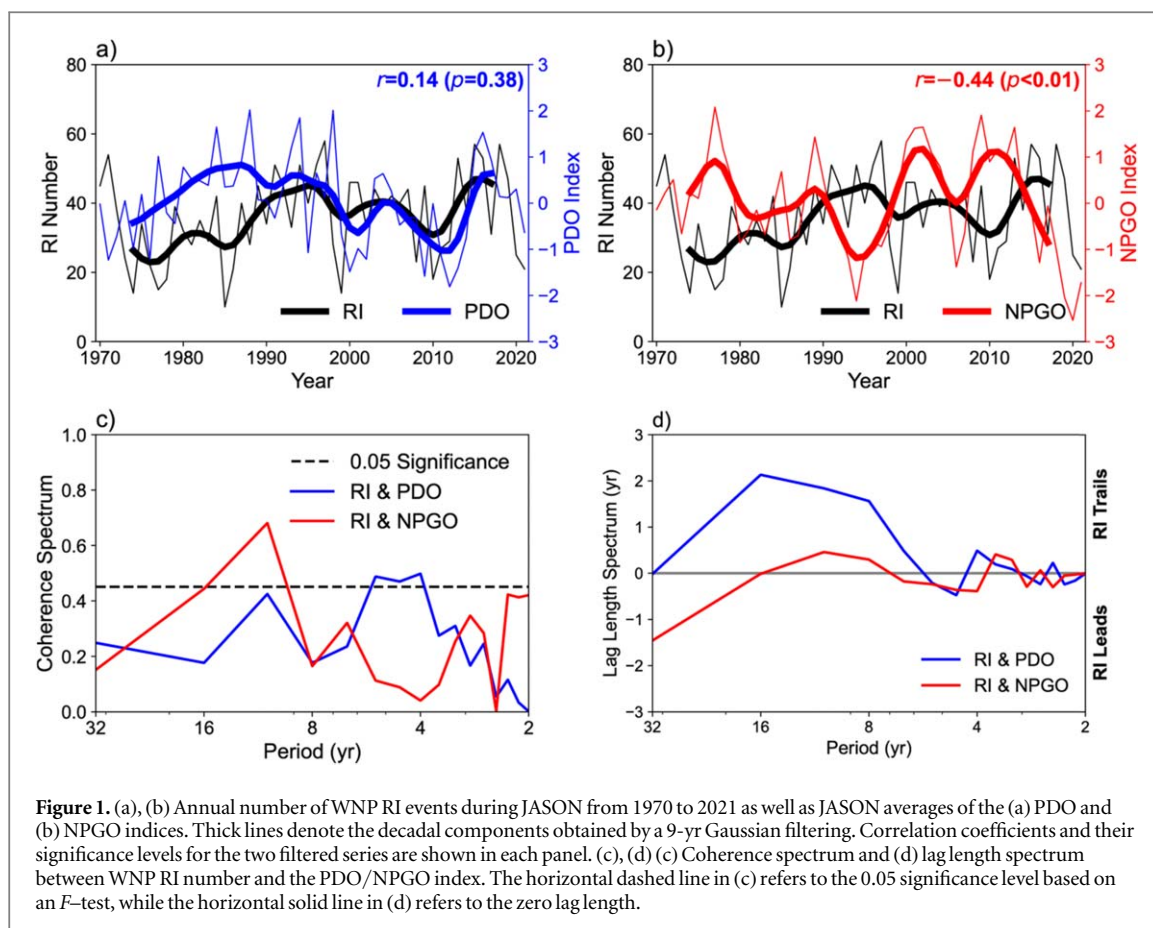
$$Y = b_0 + b_{\text{PDO}}I_{\text{PDO}} + b_{\text{NPGO}}I_{\text{NPGO}}, \quad (2)$$

where Y represents the time series of a given variable, while I_{PDO} and I_{NPGO} denote the PDO and NPGO indices, respectively. Accordingly, the regression coefficient of b_{PDO} (b_{NPGO}) measures the impact of the PDO (NPGO) on RI activity or environmental factors after linearly removing the impact of the NPGO (PDO).

The significance levels (p) of correlation coefficients (r) and partial correlation coefficients are estimated using a two-tailed Student's t -test, while significance levels of partial regression coefficients and coherence spectra are obtained through an F -test. In evaluating statistical significance, we apply the effective sample size proposed by Trenberth (1984) to minimize the influence of autocorrelation.

3. Decadal changes in RI

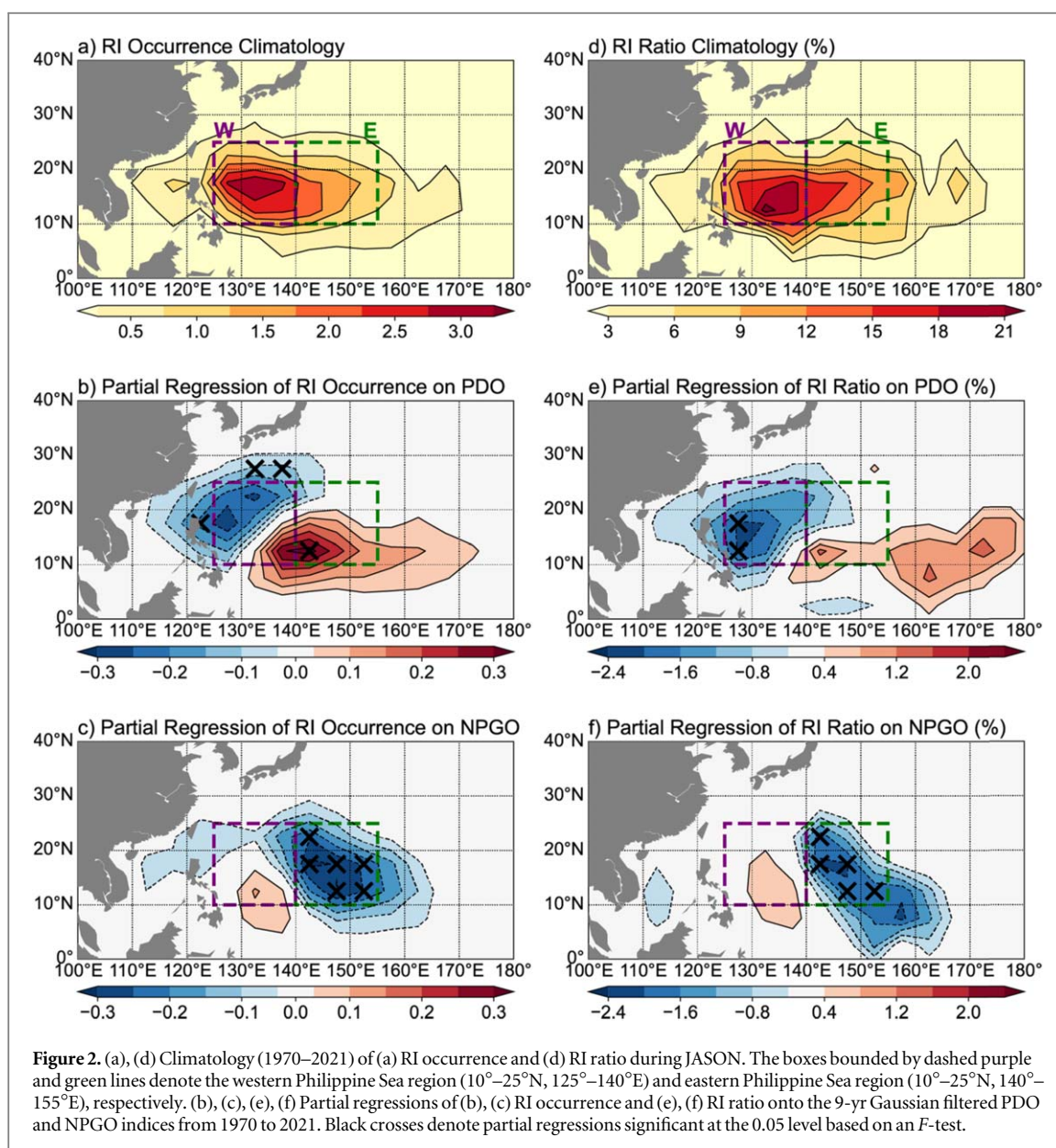
Figure 1 displays the temporal relationship between WNP RI events during JASON and the simultaneous PDO/NPGO index from 1970 to 2021. We highlight changes on decadal timescales by using a 9-yr Gaussian filter. Figure 1(a) shows only a weak decadal correlation between RI number and the PDO index ($r = 0.14$, $p = 0.38$), which can be linked to a relationship between RI and the PDO that changed sign around 1990. Decadal changes in RI number and the PDO index are nearly out of phase in the 1970s and 1980s, while they are mostly in phase since 1990. This result is inconsistent with Wang *et al* (2015), who reported a significant decadal RI-PDO correlation during May–November between 1951 and 2008. This discrepancy is possibly caused by uncertainty in TC intensity estimates during the pre-satellite era. Given the overestimation of TC intensity prior to ~ 1970 , which coincidentally corresponds to a negative phase of the PDO, there were likely a greater number of RI events recorded in the best track data. Another secondary reason for this discrepancy could be the different seasons considered in Wang *et al* (2015) and this manuscript.



By comparison, figure 1(b) displays a significant inverse relationship between RI number and the NPGO index on decadal timescales ($r = -0.44$, $p < 0.01$), implying fewer (more) RI events over the WNP during the positive (negative) phase of the NPGO. Litzow *et al* (2020) found a tendency for a strengthening negative correlation between the PDO and NPGO indices after 1988/1989. We argue that since 1990, the enhanced RI-PDO relationship is primarily induced by a strengthened PDO-NPGO coupling. When removing the NPGO's effect, the partial correlation coefficient between RI number and the PDO index is -0.23 ($p = 0.13$). The RI-PDO relationship remains insignificant, although the sign changes from positive to negative. There is a significant partial correlation coefficient between RI number and the NPGO index of -0.34 ($p = 0.03$), when the PDO's effect is removed. This implies that the PDO has relatively little influence on the RI-NPGO relationship.

Furthermore, we use a cross-spectral analysis between WNP RI number and the PDO/NPGO index to display potential coherence and phase differences as a function of periodicity (figures 1(c), (d)). RI number and the PDO index show significant coherence only on a 4–5-yr period, indicating a notable relationship on interannual timescales (figure 1(c)). Given the tight ENSO-PDO connection, it is likely that the interannual RI-PDO relationship is associated with the RI-ENSO relationship as reported in previous publications (e.g., Wang and Zhou 2008, Fudeyasu *et al* 2018). By contrast, there is a significant coherence peak between RI number and the NPGO index on a period of 8–16 yrs, confirming a robust decadal linkage (figure 1(c)). The RI-NPGO relationship is almost simultaneous on decadal timescales, because the corresponding lag length is shorter than 1 yr (figure 1(d)).

Figure 2(a) displays the climatological (1970–2021) distribution of RI occurrences during JASON over the WNP, highlighting an RI main development area east of the Philippines (10° – 25° N, 125° – 155° E). This area can be further divided into two sub-regions: the western Philippine Sea (10° – 25° N, 125° – 140° E) and the eastern Philippine Sea (10° – 25° N, 140° – 155° E). To highlight the decadal changes solely modulated by the PDO/NPGO, partial regressions onto the low-pass filtered index are analyzed in the following sections. Figure 2(b) shows the decadal influence of the PDO on WNP RI occurrences, which is characterized by a northwest-southeast dipolar structure. This feature somewhat resembles the distribution of RI occurrence anomalies during different PDO phases, as shown in Wang *et al* (2015). During the positive PDO phase, enhanced RI occurrence over the southeastern WNP has a similar magnitude and coverage to the suppressed RI occurrence over the northwestern WNP, leading to a weak modulation of the PDO on basinwide RI number (figure 2(b)).



Compared with the PDO, the decadal modulation of WNP RI by the NPGO has a distinctly different spatial distribution (figure 2(c)), with an insignificant pattern correlation coefficient of -0.21 ($p = 0.11$). During the positive NPGO phase, there is an almost basinwide suppression of WNP RI occurrence, except for a small region southeast of the Philippines where there are weak RI occurrence increases. Significant reductions in RI occurrences occur over the eastern Philippine Sea, while RI occurrence changes are not significant over the western Philippine Sea.

RI occurrence is sensitive to changes in TC occurrence. There are substantial decadal variations and long-term trends in TC occurrence location during the past decades (e.g., Kossin *et al* 2016, Wang and Toumi 2021). To minimize the influence of TC occurrence on RI activity, spatial features related to RI ratio are additionally considered. This is calculated as the proportion of RI cases to total TC cases on a grid. Figure 2(d) shows that on average, high RI ratios are observed east of the Philippines, exhibiting a nearly identical spatial structure to the RI occurrence distribution, with a pattern correlation coefficient of 0.94 ($p < 0.01$). The PDO-induced changes in RI occurrence and RI ratio are quite similar, with a pattern correlation coefficient of 0.66 ($p < 0.01$) (figures 2(b), (e)). The difference is that during positive PDO phases, RI ratios significantly decrease over the western Philippine Sea and weakly increase over the eastern Philippine Sea (figure 2(e)). This implies an average lower RI ratio over the entire WNP during positive PDO phases than during negative PDO phases, consistent with Wang *et al* (2015). Similar spatial distributions are also shown in the RI occurrence and RI ratio changes induced by the NPGO, with a greater pattern correlation coefficient of 0.81 ($p < 0.01$) than for the PDO (figures 2(c), (f)). Significant increases in RI ratio are found over the eastern Philippine Sea, while only weak changes in RI ratio are

observed over the western Philippine Sea (figure 2(f)). These results indicate that the NPGO has a very similar impact on decadal changes in RI occurrence and RI ratio over the WNP.

4. Decadal changes in environmental conditions

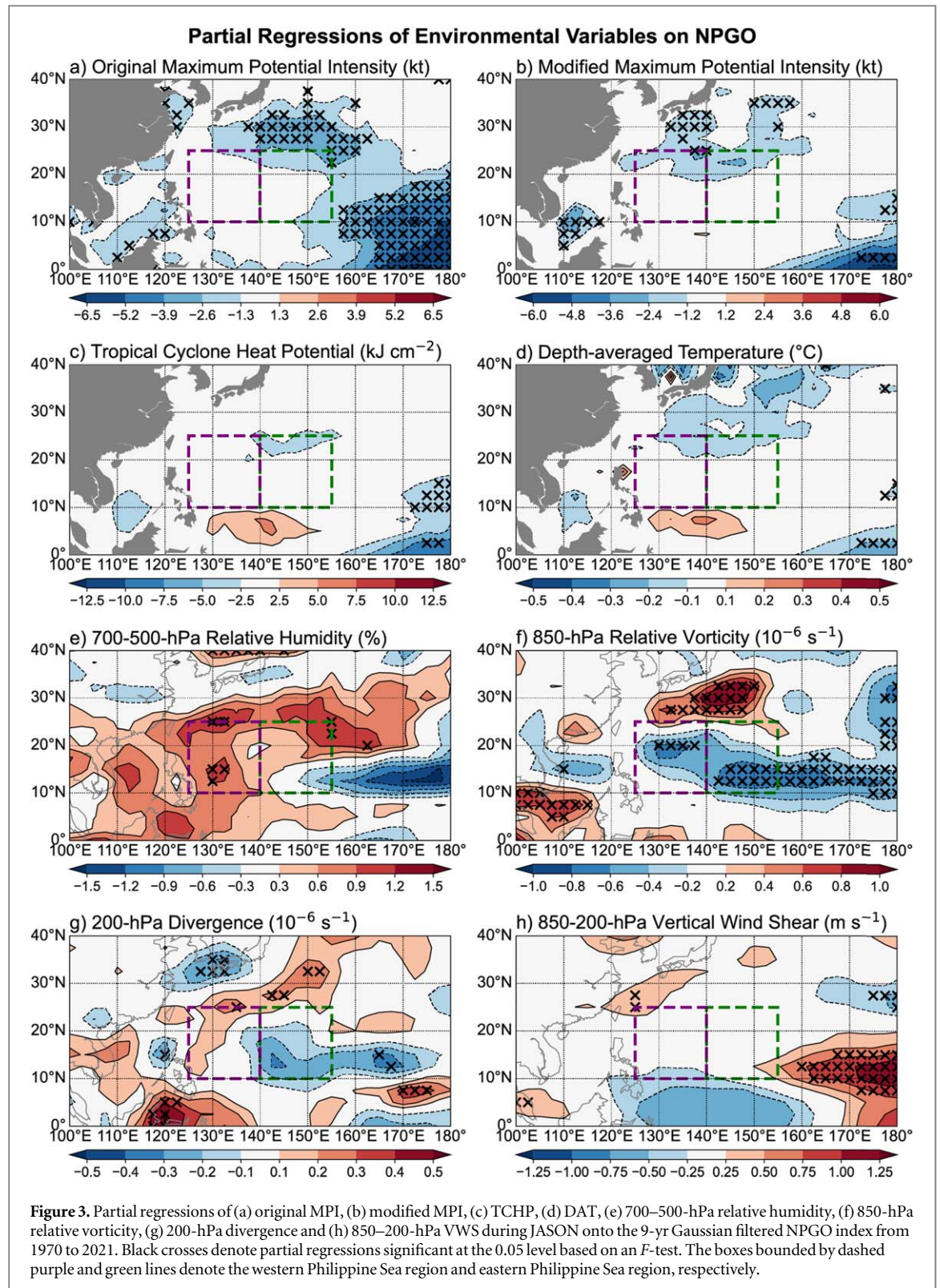
To identify possible environmental conditions responsible for decadal variations in RI, we analyze changes in seven oceanic and atmospheric variables: MPI, DAT, TCHP, 700–500-hPa relative humidity, 850-hPa relative vorticity, 200-hPa divergence and 850–200-hPa VWS (figure 3). We consider two MPI estimations here. One is the original MPI calculation proposed by Emanuel (1988), considering a TC as a heat engine in which the warm reservoir is the ocean surface and the cold reservoir is the top of the TC. The other is a modified MPI calculation where the SST is replaced by the DAT, which includes the effect of ocean cooling (Lin *et al* 2013, Lee *et al* 2019). We focus on environmental changes modulated by the NPGO, since PDO-induced environmental changes have been previously studied (e.g., Wang *et al* 2015, Zhao *et al* 2018, Zhang *et al* 2020).

During the positive NPGO phase, the area with significantly decreased MPIs concentrates over the equatorial central Pacific, the subtropical WNP and the southern part of the South China Sea (SCS), while MPIs change only slightly over the eastern and western Philippine Sea (figures 3(a), (b)). By comparison, there are almost no significant TCHP changes over the entire WNP, including over the Philippine Sea (figure 3(c)). Significantly reduced TCHPs are only found over the southeastern corner of the WNP. The changes of DAT show a similar spatial pattern as those of TCHP (figure 3(d)), given their strong correlation over the deep open ocean (Price 2009). These results imply that over the WNP, the NPGO has a much greater impact on SSTs than on sub-surface temperatures.

During the positive NPGO phase, there is a broad region with a moister lower-to-middle troposphere over the WNP, extending from the South China Sea to the subtropical WNP (figure 3(e)). Significant increases in 700–500-hPa relative humidity are observed over the western Philippine Sea, although they cover only a small portion of this region. No significant relative humidity changes are found over the eastern Philippine Sea. Similar patterns occur for NPGO-induced changes of low-level relative vorticity and upper-level divergence (figures 3(f), (g)). On average, there are decreases (increases) in 850-hPa relative vorticity and 200-hPa divergence inside (outside) of the latitudinal belt spanned by 0° – 25° N during the positive NPGO phase. However, the changes in 850-hPa relative vorticity are generally more significant than those in 200-hPa divergence, implying that the NPGO has a stronger influence at lower levels than at upper levels. There is significantly reduced vorticity but only weak divergence changes over both the western and eastern Philippine Sea. Figure 3(h) shows no significant changes in 850–200-hPa VWS over the Philippine Sea, while significantly enhanced VWSs are concentrated over the off-equatorial central Pacific (figure 3(h)). Figure 4 shows the decadal relationship between the NPGO and environmental factors averaged over the western and eastern Philippine Sea. During the positive NPGO phase, weak changes in RI occurrence over the western Philippine Sea can be linked to the offsetting influence of significantly increased 700–500-hPa humidity and significantly decreased 850-hPa vorticity. By comparison, the significant increases in RI occurrence over the eastern Philippine Sea are primarily the results of decreases in 850-hPa vorticity. The NPGO appears to modulate the other environmental variables examined here (e.g., MPI, TCHP, DAT, 200-hPa divergence and 850–200-hPa VWS) to a lesser degree (figure 4).

Figure 5 shows how the NPGO modulates vorticity and humidity changes over the western and eastern Philippine Sea. A positive NPGO is characterized by negative SSTAs over a comma-shaped area from the northeast North Pacific to the equatorial central Pacific with positive SSTAs over the North Pacific east of Japan (figure 5(a)). Compared with regressed SSTs shown in Dai *et al* (2022), partial regressions onto the NPGO exhibit strengthened and weakened SSTA magnitudes north and south of 45° N, respectively, likely caused by linearly removing the influence of the PDO. Associated with this SST pattern, the NPGO shows a dipolar structure in the 850-hPa flow over the North Pacific, similar to the NPO (figure 5(a)). During the positive NPGO phase, there is a broad anomalous anticyclonic circulation over the tropical and subtropical North Pacific, centered at 30° N, 165° W. There is a large-scale ridge extending southwestward from the center of the anticyclone to the tropical WNP. This subsequently induces negative 850-hPa vorticity over both the western and eastern Philippine Sea, suppressing RI development.

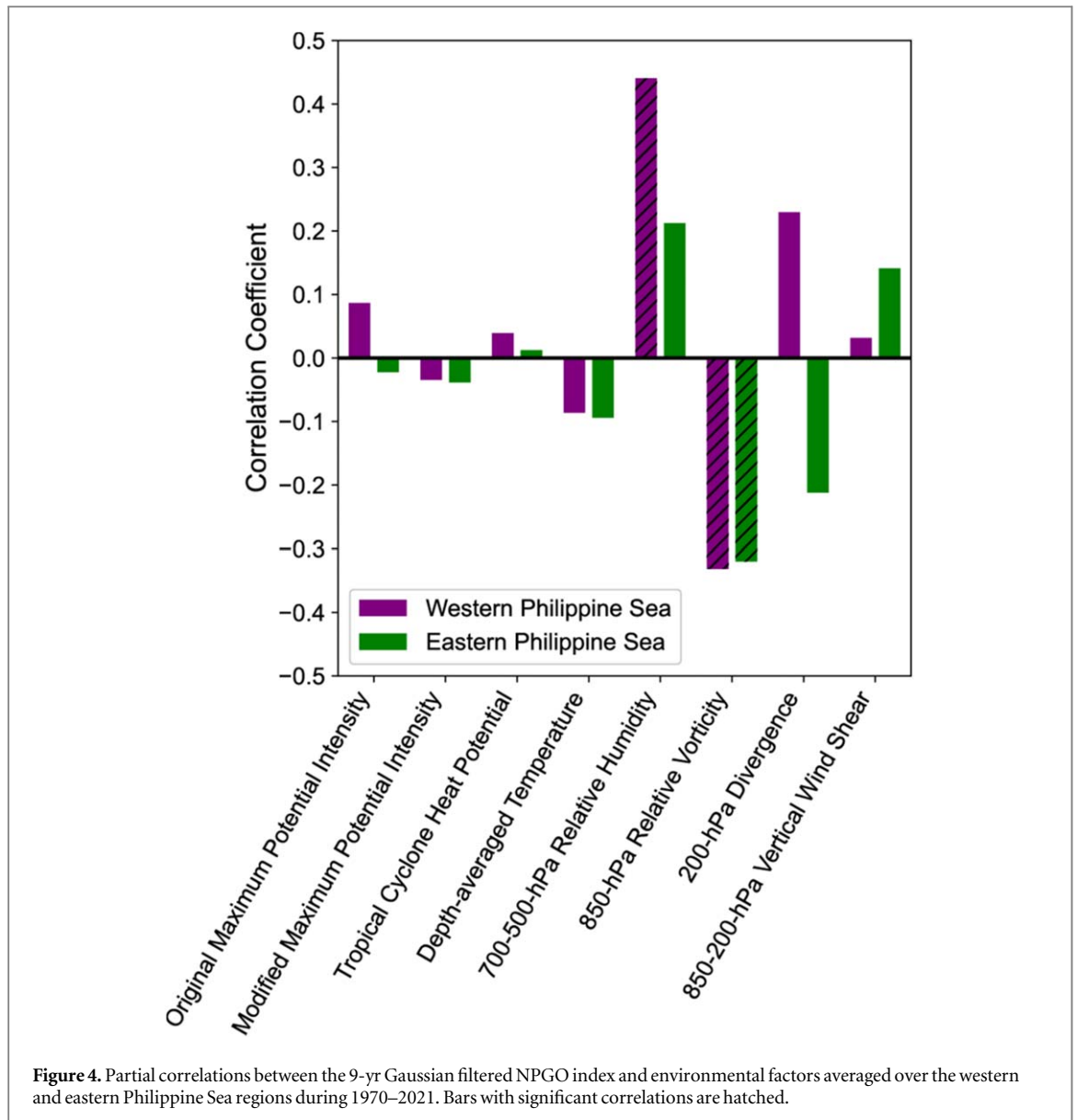
Associated with significant anomalous easterlies over the equatorial Pacific, the Walker circulation is enhanced during positive NPGO phases (figure 5(b)). There is anomalous descending motion at upper levels over the central-to-eastern equatorial Pacific (east of 150° E), resulting in negative relative humidity anomalies. By contrast, there is anomalous ascending motion throughout the troposphere over the western equatorial Pacific (west of 150° E). This leads to a moisture increase throughout the troposphere, peaking at middle levels. This increased mid-level moisture near the equator is then further transported toward the north, as shown by the anomalous moisture flux (figure 5(c)). There is significant moisture convergence over the western Philippine



Sea, causing significant humidity increases and consequently favoring RI development. By comparison, changes in moisture divergence are weak over the eastern Philippine Sea, consistent with small changes in humidity.

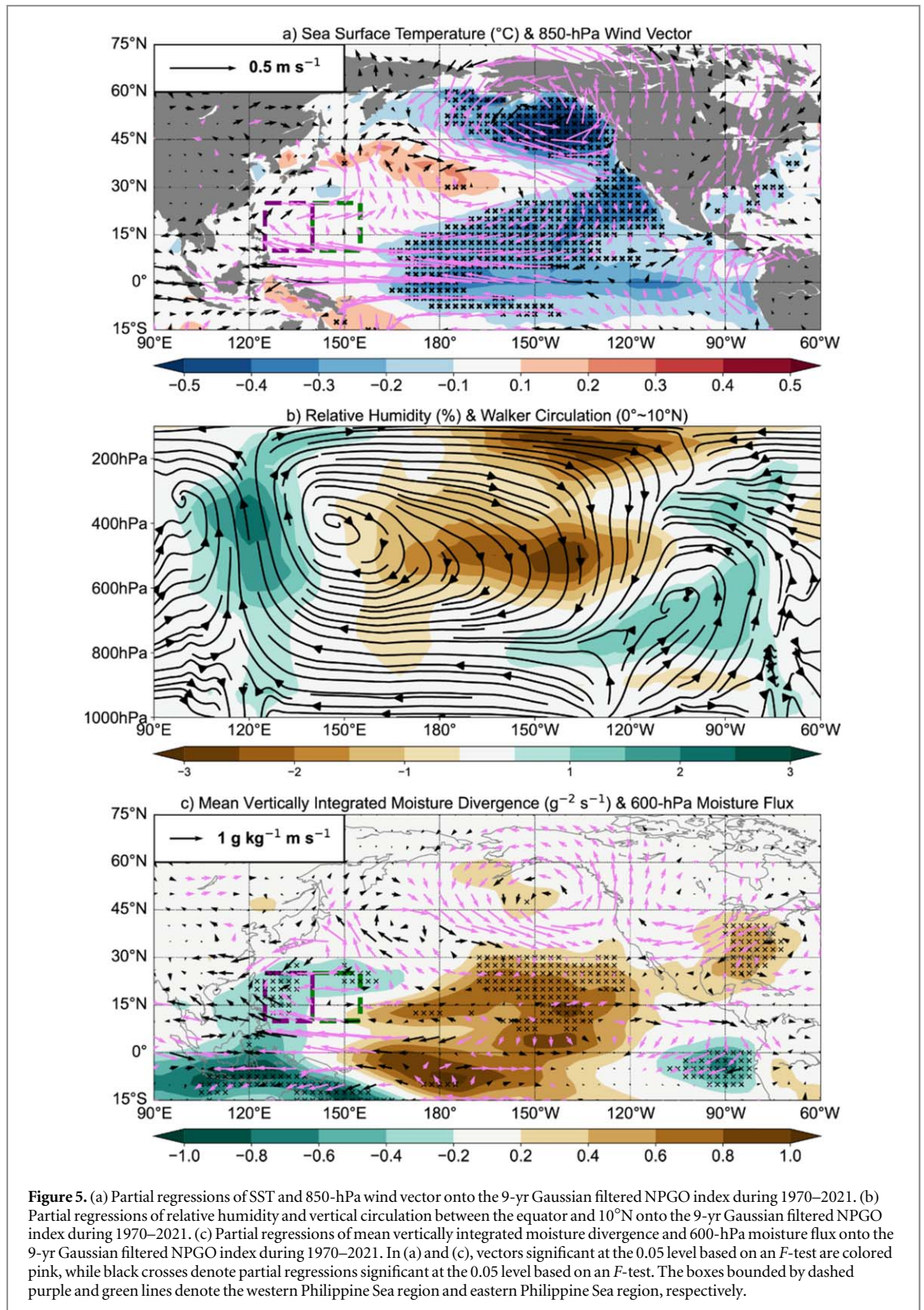
5. Summary

The decadal modulation of WNP TC RI by the NPGO and its related mechanisms are investigated in this study. There is a significant inverse relationship between WNP RI number during JASON and the simultaneous NPGO index on decadal timescales, regardless of whether the linear influence of the PDO is excluded. The average



number of WNP RI events is lower (higher) during the positive (negative) phase of the NPGO. During positive NPGO phases, RI occurrence decreases over almost the entire WNP. This pattern is distinct from the northwest-southeast structure of RI occurrence changes driven by the PDO. When focusing on the RI main development area, RI occurrences change slightly over the western Philippine Sea (10° – 25° N, 125° – 140° E) but are significantly reduced over the eastern Philippine Sea (10° – 25° N, 140° – 155° E).

The NPGO's influence on RI occurrence can be explained by variations in large-scale environmental variables. In general, over the Philippine Sea, 850-hPa relative vorticity and 700–500-hPa relative humidity play a more important role in modulating RI occurrence than other factors (e.g., MPI, TCHP, 200-hPa divergence and 850–200-hPa VWS) do. During the positive NPGO phase, there is significantly decreased vorticity and significantly increased humidity over the western Philippine Sea. These effects appear to largely balance each other out, leading to only weak variations in RI occurrence. Since other environmental factors change little, the RI-suppressing effect of significantly decreased vorticity dominates the eastern Philippine Sea, resulting in a significant RI occurrence reduction. These vorticity and humidity changes are further linked to anomalous circulations induced by the NPGO. During the positive NPGO phase, the Philippine Sea is located underneath an anomalous large-scale low-level anticyclone covering the tropical and subtropical North Pacific. Associated with anomalous equatorial easterlies, an enhanced Walker circulation induces anomalous ascending motion over the western equatorial Pacific, increasing tropospheric humidity. This increased moisture is further transported into the western Philippine Sea. By contrast, anomalous moisture transport changes are not significant over the eastern Philippine Sea.



Our results highlight the modulation of WNP RI activity by the NPGO on decadal timescales. Given that the NPGO has taken the place of the PDO as the primary mode of North Pacific variability during recent decades (Bond *et al* 2003, Litzow *et al* 2020), decadal WNP RI activity can be predicted based on projections of future NPGO phase changes. One caveat of our study is that our results are obtained from a statistical analysis of a limited number of samples. Our findings will be verified by numerical experiments using forcings of different PDO/NPGO phases in future work.

Acknowledgments

This work was jointly funded by the National Natural Science Foundation of China (42192554, 61827901, 42175007, 41905001 and 42192554) and the Meteorological Research Program of Guangxi Province of China (2023ZL04). Klotzbach would like to acknowledge financial support from the G Unger Vetlesen Foundation.

Data availability statement

The data cannot be made publicly available upon publication because they are not available in a format that is sufficiently accessible or reusable by other researchers. The data that support the findings of this study are available upon reasonable request from the authors.

ORCID iDs

Jinjie Song  <https://orcid.org/0000-0003-3948-8894>

References

- Bond N A and Harrison D E 2000 The Pacific decadal oscillation, air-sea interaction and central north Pacific winter atmospheric regimes *Geophys. Res. Lett.* **27** 731–4
- Bond N A, Overland J E, Spillane M and Stabeno P J 2003 Recent shifts in the state of the north Pacific *Geophys. Res. Lett.* **30** 2183
- Cai W, van Rensch P, Cowan T and Hendon H H 2011 Teleconnection pathways of ENSO and the IOD and the mechanisms for impacts on Australian rainfall *J. Climate* **24** 3910–23
- Chhak K C, D Lorenzo E, Schneider N and Cummins P F 2009 Forcing of low-frequency ocean variability in the northeast Pacific *J. Climate* **22** 1255–76
- Chu P-S and Murakami H 2022 *Climate Variability and Tropical Cyclone Activity* (New York: Cambridge University Press) p 320
- Dai Y, Wang B, Wei N, Song J and Duan Y 2022 How has the north Pacific gyre oscillation affected peak season tropical cyclone genesis over the western north Pacific from 1965 to 2020? *Environ. Res. Lett.* **17** 104016
- Di Lorenzo E *et al* 2008 North Pacific gyre oscillation links ocean climate and ecosystem change *Geophys. Res. Lett.* **35** 2–7
- Di Lorenzo E, Cobb K M, Furtado J C, Schneider N, Anderson B T, Bracco A, Alexander M A and Vimont D J 2010 Central Pacific El Niño and decadal climate change in the north Pacific *Nat. Geosci.* **3** 762–5
- Ding R Q, Li J P, Tseng Y-H, Sun C and Guo Y P 2015 The Victoria mode in the north Pacific linking extratropical sea level pressure variations to ENSO *J. Geophys. Res. Atmos.* **120** 27–45
- Dong Z, Zhou F, Zheng Z and Fang K 2022 Increased amplitude of the north Pacific gyre oscillation towards recent: evidence from tree-ring-based reconstruction since 1596 *Int. J. Climatol.* **42** 6403–12
- Emanuel K A 1988 The maximum intensity of hurricanes *J. Atmos. Sci.* **45** 1143–55
- Emanuel K A 2000 A statistical analysis of tropical cyclone intensity *Mon. Wea. Rev.* **128** 1139–52
- Fudeyasu H, Ito K and Miyamoto Y 2018 Characteristics of tropical cyclone rapid intensification over the western north Pacific *J. Climate* **31** 8917–30
- Ge X, Shi D and Guan L 2018 Monthly variations of tropical cyclone rapid intensification ratio in the western north Pacific *Atmos. Sci. Lett.* **9** e814
- Guo Y-P and Tan Z-M 2021 Influence of different ENSO types on tropical cyclone rapid intensification over the western north Pacific *J. Geophys. Res.* **126** e2020JD033059
- Ham Y-G, Kug J-S, Park J-Y and Jin F-F 2013 Sea surface temperature in the north tropical Atlantic as a trigger for El Niño/Southern Oscillation events *Nat. Geosci.* **6** 112–6
- Hersbach H *et al* 2020 The ERA5 global reanalysis *Quart. J. Roy. Meteor. Soc.* **146** 1999–2049
- Kaplan J and DeMaria M 2003 Large-scale characteristics of rapidly intensifying tropical cyclones in the north Atlantic basin *Wea. Forecasting* **18** 1093–108
- Kaplan J, DeMaria M and Knaff J A 2010 A revised tropical cyclone rapid intensification index for the Atlantic and East Pacific basins *Wea. Forecasting* **25** 220–41
- Kim S H, Moon I J and Chu P S 2020 An increase in global trends of tropical cyclone translation speed since 1982 and its physical causes *Environ. Res. Lett.* **15** 094084
- Knaff J A, Sampson C R and Musgrave K D 2018 An operational rapid intensification prediction aid for the western north Pacific *Wea. Forecasting* **33** 799–811
- Knapp K R, Kruk M C, Levinson D H, Diamond H J and Neumann C J 2010 The International Best Track Archive for Climate Stewardship (IBTrACS) *Bull. Amer. Meteor. Soc.* **91** 363–76
- Kossin J P, Emanuel K A and Camargo S J 2016 Past and projected changes in western north Pacific tropical cyclone exposure *J. Climate* **29** 5725–39
- Kowch R and Emanuel K A 2015 Are special processes at work in the rapid intensification of tropical cyclones? *Mon. Wea. Rev.* **143** 878–82
- Lee C Y, Tippet M K, Sobel A H and Camargo S J 2016 Rapid intensification and the bimodal distribution of tropical cyclone intensity *Nat. Commun.* **7** 10625
- Lee W, Kim S-H, Chu P-S, Moon I-J and Soloviev A V 2019 An index to better estimate tropical cyclone intensity change in the western north Pacific *Geophys. Res. Lett.* **46** 8960–8
- Li Y, Tang Y, Toumi R and Wang S 2022 Revisiting the definition of rapid intensification of tropical cyclones by clustering the initial intensity and inner-core size *J. Geophys. Res.* **127** e2022JD036870
- Lin I-I, Black P, Price J F, Yang C-Y, Chen S S, Lien C-C, Harr P, Chi N-H, Wu C-C and D'Asaro E A 2013 An ocean coupling potential intensity index for tropical cyclones *Geophys. Res. Lett.* **40** 1878–82

- Litzow M A, Hunsicker M E, Bond N A, Burke B J, Cunningham C J, Gosselin J L, Norton E L, Ward E J and Zador S G 2020 The changing physical and ecological meanings of north pacific ocean climate indices *Proc. Natl. Acad. Sci. U.S.A.* **117** 7665–71
- Mantua N J, Hare S R, Zhang Y, Wallace J M and Francis R C 1997 A Pacific interdecadal climate oscillation with impacts on salmon production *Bull. Amer. Meteor. Soc.* **78** 1069–79
- Newman M *et al* 2016 The pacific decadal oscillation, revisited *J. Climate* **29** 4399–427
- Price J F 2009 Metrics of hurricane–ocean interaction: vertically-integrated or vertically-averaged ocean temperature? *Ocean Sci.* **5** 351–68
- Qin N, Wu L, Liu Q and Zhou X 2023 Driving forces of extreme updrafts associated with convective bursts in the eyewall of a simulated tropical cyclone *J. Geophys. Res.* **128** e2022JD037061
- Rayner N A, Parker D E, Horton E B, Folland C K, Alexander L V, Rowell D P, Kent E C and Kaplan A 2003 Global analyses of sea surface temperature, sea ice, and night marine air temperature since the late nineteenth century *J. Geophys. Res.* **108** 4407
- Rogers J C 1981 The North Pacific Oscillation *J. Clim.* **1** 39–57
- Saji N H and Yamagata T 2003 Structure of SST and surface wind variability during indian ocean dipole mode events: COADS observations *J. Climate* **16** 2735–51
- Shi D, Ge X, Peng M and Li T 2020 Characterization of tropical cyclone rapid intensification under two types of el niño events in the western north pacific *Int. J. Climatol.* **40** 2359–72
- Shu S, Ming J and Chi P 2012 Large-scale characteristics and probability of rapidly intensifying tropical cyclones in the western north pacific basin *Wea. Forecasting* **27** 411–23
- Song J, Duan Y and Klotzbach P J 2020 Increasing trend in rapid intensification magnitude of tropical cyclones over the western north pacific *Environ. Res. Lett.* **15** 084043
- Sullivan A, Luo J–J, Hirst A C, Bi D, Cai W and He J 2016 Robust contribution of decadal anomalies to the frequency of central–Pacific El Niño *Sci. Rep.* **6** 38540
- Trenberth K E 1984 Some effects of finite sample size and persistence on meteorological statistics *Part I: Autocorrelations. Mon. Wea. Rev.* **112** 2359–68
- Walsh K J *et al* 2016 Tropical cyclones and climate change *Wiley Interdiscip. Rev.: Climate Change* **7** 65–89
- Wang B and Zhou X 2008 Climate variation and prediction of rapid intensification in tropical cyclones in the western north pacific *Meteorol. Atmos. Phys.* **99** 1–16
- Wang S and Toumi R 2021 Recent migration of tropical cyclones toward coasts *Science* **371** 514–7
- Wang X, Wang C, Zhang L and Wang X 2015 Multidecadal variability of tropical cyclone rapid intensification in the western north pacific *J. Climate* **28** 806–3820
- Wang Y–F, Yang B and Tan Z–M 2023 Cloud-radiation feedback facilitates secondary eyewall formation of tropical cyclones *J. Geophys. Res.* **128** e2022JD038205
- Wu Q, Wang X and Tao L 2020 Interannual and interdecadal impact of western north pacific subtropical high on tropical cyclone activity *Clim. Dyn.* **54** 2237–48
- Yi D L, Zhang L and Wu L 2015 On the mechanisms of decadal variability of the north pacific gyre oscillation over the 20th century *J. Geophys. Res. Oceans* **120** 6114–29
- Zhang D, Zhang J, Shi L and Yao F 2020 Interdecadal changes of characteristics of tropical cyclone rapid intensification over western north pacific *IEEE Access* **8** 15781–91
- Zhang W, Leung Y and Min J 2013 North pacific gyre oscillation and the occurrence of western north pacific tropical cyclones *Geophys. Res. Lett.* **40** 5205–11
- Zhao H, Duan X, Raga G B and Klotzbach P J 2018 Changes in characteristics of rapidly intensifying western north pacific tropical cyclones related to climate regime shifts *J. Climate* **31** 8163–79
- Zhu J, Guan Z and Wang X 2022 Variations of summertime ssta independent of enso in the maritime continent and their possible impacts on rainfall in the asian–australian monsoon region *J. Climate* **35** 7949–64
- Zuo H, Balmaseda M A, Tietsche S, Mogensen K and Mayer M 2019 The ECMWF operational ensemble reanalysis-analysis system for ocean and sea-ice: a description of the system and assessment *Ocean Sci.* **15** 779–808